DOI: 10.1002/chem.200800763

A Comparison of the Magnetic Structures of $KMn_4(PO_4)_3$ and $KCo_4(PO_4)_3$ Based on the Connectivity of the Coordination Polyhedra

María Luisa López,*[a] Abdelaali Daidouh,[a] Carlos Pico,[a] Juan Rodríguez-Carvajal,[b] and María Luisa Veiga[a]

Abstract: The crystal structures of $KMn_4(PO_4)_3$ and $KCo_4(PO_4)_3$ have been determined by neutron diffraction at room temperature. Both compounds are orthorhombic with similar cell parameters, but they crystallize in different space groups, *Pnam* for the Mn phosphate and *Pnnm* for the Co analogue. On the basis of the metal cation polyhedra and their connectivity, the crystal structures have been rationalised, which allow interpretation of the main magnetic interactions between them. Magnetic measurements show ferromagnetic behaviour for the Co compound, whereas in the Mn derivative antiferromagnetism is observed. Both magnetic structures are described and qualitatively analysed in terms of superexchange and super–superexchange interactions.

Keywords: cobalt · magnetic structures · manganese · materials science · phosphates

Introduction

Phosphates of transition metal elements in low oxidation states have aroused great interest in recent years.[1–3] The phosphate frameworks are able to stabilise metal-rich phases due to the relatively high charge of the PO_4^{3-} tetrahedral basic units, which favours the formation of anionic frameworks with high mechanical, chemical, and thermal stabilities. In particular, the complex structural chemistry of several orthophosphates of the general formula $AM_4(PO_4)_3$ (A = alkali metal, M = divalent metal cation) has been studied for many years,[4–10] and different crystal structures have been described.

Members of this series of phosphates show orthorhombic symmetries and quite similar unit-cell parameters, which mainly depend on the cation sizes. Nevertheless, very noticeable differences in the metal coordination polyhedra and their connectivity are encountered, the main consequence of which is wide variation in their magnetic properties. In this context, some of us have recently reported the crystal and magnetic structures of the nickel derivative of this series of compounds, $KNi_4(PO_4)_3$.[10] In this phase, three magnetic crystallographic sites of Ni^{2+} ions interact through common oxygen atoms of the phosphate groups, giving rise to ferromagnetic (FM) and antiferromagnetic (AFM) couplings. The resulting macroscopic behaviour is FM.

The structural similarity between the nickel and manganese derivatives was suggested by Yakubobich et al.,[7] although there are some differences between the two structures that are reflected in their different space groups. A key difference is the pentagonal arrangement of the Mn^{2+} ions, as is discussed later, which is not present in the Ni^{2+} compound. This feature must be taken into account when the respective magnetic properties are analysed.

We report herein the room temperature crystal structure refinements and the low-temperature magnetic structures of $KM_4(PO_4)_3$ (M = Mn, Co), as obtained by high-resolution neutron powder diffraction (NPD) analysis. On the basis of these results, the magnetic structures are interpreted in terms of possible M-O-M superexchange and super–superexchange (M-O-O-M) interactions mediated by isolated phosphate groups. The analogies and differences between the crystal structures are discussed on the basis of the coordination polyhedra of the metal cations, and these permit rationalisation of their respective magnetic behaviours. Moreover, the magnetic single-ion anisotropy of the Co^{2+} elec-

[a] Dr. M. L. López, Dr. A. Daidouh, Dr. C. Pico, Dr. M. L. Veiga
Química Inorgánica I Facultad de Ciencias Químicas
Universidad Complutense de Madrid
Ciudad Universitaria s/n, 28040 Madrid (Spain)
Fax: (+34) 913-944-352
E-mail: marisal@quim.ucm.es

[b] Dr. J. Rodríguez-Carvajal
Institut Max Von Laue-Paul Langevin (ILL)
6 rue Jules Horowitz, BP 156
38042 Grenoble Cedex 9 (France)

tronic configuration may explain its contrasting behaviour compared to that of the isomorphous Ni^{2+} phosphate.

Results and Discussion

Crystal structures: Structural refinements of $KM_4(PO_4)_3$ (M = Mn, Co) were carried out from high-resolution NPD patterns collected at room temperature with $\lambda = 1.911$ Å. Rietveld refinement for the manganese derivative was carried out in the *Pnam* space group, taking the cell parameters reported for a single-crystal specimen by Yakubovich et al.[7] as a starting point. For this phosphate, the minor Mn_2O_3 impurity was included as a second crystallographic phase in the refinements. The cobalt compound was refined in the *Pnnm* space group, being isostructural with the nickel phosphate of the same stoichiometry, the crystal and magnetic structures of which have already been published by some of us.[10]

The agreement between the observed and calculated patterns was satisfactory, and the Mn and Co Rietveld plots are shown in Figures 1 and 2, respectively. The structural parameters calculated in the refinement are gathered in Table 1. The final refined positional and thermal parameters are given in Tables 2 and 3, and the main interatomic distances, angles, and bond valence sums (BVS) around the cations are listed in Tables 4 and 5.

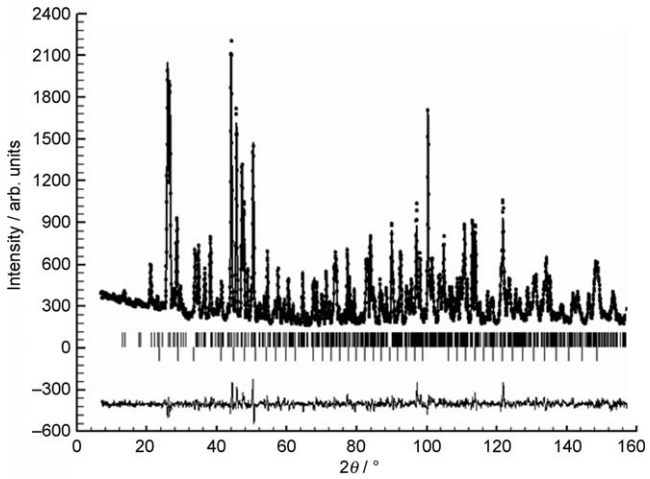

Figure 1. Observed (circles), calculated (solid line), and difference (at the bottom) neutron diffraction (D1A, ILL) profiles for $KMn_4(PO_4)_3$ at room temperature. Vertical marks correspond to the position of the allowed reflections for the crystallographic structure. The second series of tick marks corresponds to the Bragg reflections of the Mn_2O_3 impurity phase.

On the basis of these results, the different cation polyhedra can be described as follows. In both phosphates, the potassium cations adopt a six-fold coordination in a distorted trigonal prism. Three independent crystallographic sites for M (M = Mn, Co) and the phosphorus atoms were found. In the first compound, two manganese atoms are arranged

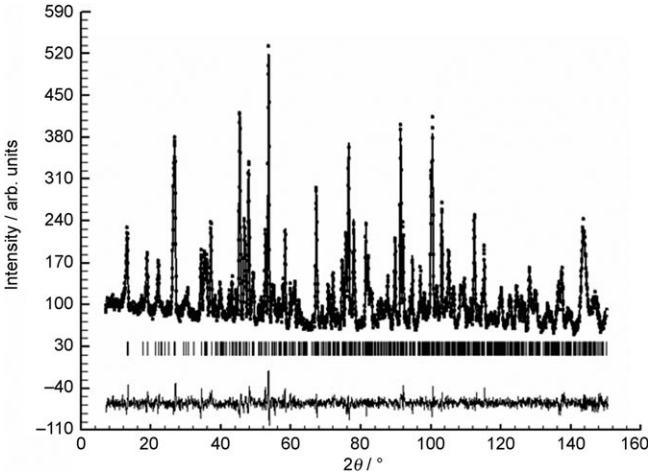

Figure 2. Observed (circles), calculated (solid line), and difference (at the bottom) neutron diffraction (D1A, ILL) profiles for $KCo_4(PO_4)_3$ at room temperature. Vertical marks correspond to the position of the allowed reflections for the crystallographic structure.

Table 1. Cell parameters and agreement factors of full-profile refinements from the neutron diffraction pattern of $KM_4(PO_4)_3$ at room temperature.

M	Mn	Co
space group	*Pnam*	*Pnnm*
a [Å]	9.985145(13)	9.62897(9)
b [Å]	16.049761(17)	16.48179(17)
c [Å]	6.558394(8)	6.16644(6)
V [Å^3]	1051.04(28)	978.63(17)
reflections	661	597
parameters	61	61
R_p (%) $= \Sigma \mid y_{i,obs} - y_{i,calc} \mid / \Sigma y_{i,obs}$	10.5	12.0
R_{wp} (%) $= [\Sigma w_i \{y_{i,obs} - y_{i,calc}\}^2 / \Sigma w_i [y_{i,obs}]^2]^{1/2}$	11.7	12.6
R_B (%) $= [\Sigma \mid I_{obs} - I_{calc} \mid] / \Sigma I_{obs}$	5.58	4.20
$\chi^2 = \Sigma w_i \{y_{i,obs} - y_{i,calc}\}^2 / (N - P + C)$	3.537	1.52

Table 2. Final refined positional and thermal parameters from the neutron diffraction pattern (D1A) of $KMn_4(PO_4)_3$ at room temperature.

Atom	Site	x	y	z	B_{iso} [Å^2]
K	4*c*	0.2369(8)	0.2832(5)	0.25	1.61(18)
Mn1	4*c*	0.4685(6)	0.8666(4)	0.25	1.12(17)
Mn2	4*c*	0.0745(7)	0.8749(4)	0.25	0.55(12)
Mn3	8*d*	0.2461(5)	0.0505(3)	0.0025(6)	0.12(7)
P1	4*c*	0.0244(4)	0.4382(3)	0.25	0.40(8)
P2	4*c*	0.4480(4)	0.4476(3)	0.25	0.01(11)
P3	4*c*	0.2964(4)	0.7226(3)	0.25	0.45(9)
O1	4*c*	0.1163(5)	0.5201(3)	0.25	0.71(9)
O2	4*c*	0.3753(5)	0.0265(3)	0.25	1.34(11)
O3	8*d*	0.0505(3)	0.38931(17)	0.0610(5)	0.48(7)
O4	4*c*	0.1059(4)	0.0521(3)	0.25	0.31(8)
O5	4*c*	0.4020(4)	0.5390(3)	0.25	0.85(11)
O6	8*d*	0.3933(4)	0.40765(20)	0.0577(5)	0.99(7)
O7	4*c*	0.2537(5)	0.8149(3)	0.25	0.57(9)
O8	8*d*	0.2447(4)	0.6768(2)	0.0587(5)	1.33(7)
O9	4*c*	0.4482(4)	0.7278(3)	0.25	0.69(10)

in distorted trigonal bipyramids, labelled Mn1 and Mn2, and the third one is in a square pyramid, Mn3. The three kinds of Co atoms are arranged in distorted trigonal bipyramids,

labelled Co1, and in octahedral coordination environments, labelled as Co2 and Co3. The phosphorus atoms form slightly distorted tetrahedra. From the data gathered in Tables 4 and 5, it can be seen that the mean bond lengths and the BVS values are in good agreement with the sum of the ionic radii[13] and the calculated valences for all atoms, respectively.

Table 3. Final refined positional and thermal parameters from the neutron diffraction pattern (D1A) of $KCo_4(PO_4)_3$ at room temperature.

Atom	Site	x	y	z	B_{iso} [Å^2]
K	4*g*	0.2976(11)	0.4640(7)	0.0	2.6(2)
Co1	4*g*	0.5314(14)	0.0941(8)	0.0	0.7(2)
Co2	4*g*	0.9729(15)	0.1408(8)	0.0	1.0(3)
Co3	8*h*	0.2439(10)	0.2528(13)	0.2000(7)	1.34(18)
P1	4*g*	0.0427(7)	0.3358(4)	0.0	0.91(12)
P2	4*g*	0.4534(7)	0.2804(4)	0.0	0.12(11)
P3	4*g*	0.2087(6)	0.0368(4)	0.0	0.28(11)
O	4*g*	0.8811(6)	0.3218(4)	0.0	0.79(11)
O2	4*g*	0.6134(6)	0.2760(3)	0.0	0.66(12)
O3	8*h*	0.5907(4)	0.1208(3)	0.2983(7)	1.15(8)
O4	4*g*	0.3906(6)	0.1940(4)	0.0	1.00(11)
O5	4*g*	0.1100(7)	0.2465(4)	0.0	1.45(14)
O6	4*g*	0.8616(7)	0.0440(4)	0.0	1.76(14)
O7	8*h*	0.1660(4)	0.0889(3)	0.1987(7)	1.38(8)
O8	8*h*	0.9002(4)	0.1790(2)	0.7068(7)	1.00(8)
O9	4*g*	0.3668(7)	0.0207(4)	0.0	1.76(14)

The projections of the overall structures in the *b*-*c* plane (Figure 3a, b) show their complexity, and they can be viewed as being made up of $[M_4(PO_4)_3]$ groups forming tunnels parallel to the *a* axis, in which the potassium cations are located. The M-O framework is the primary focus of this description in order to later rationalise the respective magnetic behaviours.

For $KMn_4(PO_4)_3$, abbreviated as KMn hereafter, the framework defined by the transition metal polyhedra can be decomposed into two different fragments for clarity. One of them is defined by the Mn3 (yellow) arrangement, which forms one-dimensional chains of edge-sharing square pyramids that extend along the *c* axis. The second fragment is built-up of the Mn2 (green) and Mn1 (pink) polyhedra, which share two contiguous corners giving rise to zigzag chains along the *a* axis (Figure 3c). Each link of the chains is formed by two alternating pairs of Mn1-O-Mn2. Both fragments collapse around tetrahedral $[PO_4]$ groups giving rise to pentagonal rings formed by neighbouring Mn^{2+} ions that lie parallel to the *b* axis. These pentagonal rings defined by manganese ions (i.e., Mn1-Mn2-Mn3-Mn1-Mn2) give rise to parallel sheets, which are joined by $[PO_4]$ anions along the *b* axis (see Figure 3c). Visualisation of these structural features is essential to interpret the overall magnetic behaviour of this compound.

As has already been mentioned, $KCo_4(PO_4)_3$, abbreviated as KCo, is isostructural with the nickel compound;[10] therefore, we only point out here the main similarities and differences of this phosphate with respect to KMn that are pertinent to interpreting their magnetic structures.

As a consequence of the cation sizes and the arrangement of the cation polyhedra in these phosphates, their unit cell metrics are very similar. In this context, Figures 3a), b) show the *bc* projections of these structures, in which the resemblances between them can clearly be seen. Sheets of Mn or Co and P polyhedra parallel to the (100) planes of the structures are observed, although the Co2 and Co3 atoms are six-coordinated whereas all of the Mn atoms are five-coordinated by oxygen.

On the other hand, Figure 3c), d) show the perpendicular perspectives of the above structures, which reveal the main differences in the connectivities of their polyhedra. For

Table 4. Main bond lengths [Å], angles [°], and bond valence sums around the cations for $KMn_4(PO_4)_3$.

KO_6					
K–O3	2.811(8) ×2	K–O6	2.832(8) ×2	K–O8	2.660(6) ×2
mean	2.767(3)				
Shannon	2.795				
valence sum	1.101(9)				
$P1O_4$		$P2O_4$		$P3O_4$	
P1–O1	1.603(7)	P2–O4	1.577(6)	P3–O7	1.542(7)
P1–O2	1.593(6)	P2–O5	1.537(7)	P3–O8	1.538(4) ×2
P1–O3	1.490(4) ×2	P2–O6	1.517(4) ×2	P3–O9	1.518(6)
mean	1.544(2)	mean	1.536(6)	mean	1.533(7)
Shannon	1.534	Shannon	1.534	Shannon	1.534
valence sum	4.925(34)	valence sum	4.980(35)	valence sum	5.011(36)
$Mn1O_5$		$Mn2O_5$		$Mn3O_5$	
Mn1–O1	2.342(8)	Mn2–O5	2.208(8)	Mn3–O1	2.206(6)
Mn1–O3	2.081(3) ×2	Mn2–O6	2.110(4) ×2	Mn3–O2	2.109(5)
Mn1–O7	2.300(8)	Mn2–O7	2.032(8)	Mn3–O4	2.144(5)
Mn1–O9	2.237(8)	Mn2–O9	2.075(8)	Mn3–O5	2.228(5)
mean	2.208(9)	mean	2.107(3)	Mn3–O8	2.070(6)
Shannon	2.129	Shannon	2.129	mean	2.151(4)
valence sum	1.688(11)	valence sum	2.147(18)	Shannon	2.1501(26)
				valence sum	1.907(13)
$Mn1O_5$		$Mn2O_5$		$Mn3O_5$	
O1-Mn1-O3	84.2(3) ×2	O5-Mn2-O6	87.0(3) ×2	O1-Mn3-O2	98.6(2)
O1-Mn1-O7	149.9(5)	O5-Mn2-O7	167.6(5)	O1-Mn3-O5	80.6(3)
O1-Mn1-O9	145.3(5)	O5-Mn2-O9	92.1(4)	O1-Mn3-O8	92.7(3)
O3-Mn1-O3	156.3(3)	O6-Mn2-O6	144.2(3)	O2-Mn3-O4	79.6(4)
O3-Mn1-O7	89.9(4) ×2	O6-Mn2-O7	89.2(4) ×2	O2-Mn3-O8	108.4(3)
O3-Mn1-O9	100.7(4) ×2	O6-Mn2-O9	107.7(4) ×2	O4-Mn3-O5	97.2(2)
O7-Mn1-O9	64.8(4)	O7-Mn2-O9	100.3(5)	O4-Mn3-O8	100.5(3)
				O5-Mn3-O8	88.1(3)

Table 5. Main bond lengths [Å], angles [°], and bond valence sums around the cations for $KCo_4(PO_4)_3$.

KO_6					
K–O3	2.733(11) ×2	K–O7	2.795(10) ×2	K–O8	2.856(11) ×2
mean	2.7947(43)				
Shannon	2.795				
valence sum	1.010(12)				
$P1O_4$		$P2O_4$		$P3O_4$	
P1–O1	1.573(9)	P2–O2	1.542(9)	P3–O6	1.494(9)
P1–O3	1.507(6) ×2	P2–O4	1.547(9)	P3–O7	1.552(6) ×2
P1–O5	1.608(9)	P2-O-8	1.529(5) ×2	P3–O9	1.545(9)
mean	1.5490(38)	mean	1.5356(38)	mean	1.5356(38)
Shannon	1.5344	Shannon	1.5344	Shannon	1.5344
valence sum	4.840(48)	valence sum	4.995(53)	valence sum	4.995(53)
$Co1O_5$		$Co2O_6$		$Co3O_6$	
Co1–O3	1.976(7) ×2	Co2–O5	2.186(15)	Co3–O1	2.049(10)
Co1–O4	2.133(15)	Co2–O6	1.922(15)	Co3–O2	2.015(10)
Co1–O9	1.994(15)	Co2–O7	2.385(13) ×2	Co3–O4	2.106(10)
Co1–O9	2.131(15)	Co2–O8	2.038(8) ×2	Co3–O5	2.163(10)
mean	2.041(5)	mean	2.159(5)	Co3–O7	2.007(12)
				Co3–O8	2.515(11)
Shannon	2.098	Shannon	2.098	mean	2.098
valence sum	1.980(27)	valence sum	1.891(28)	Shannon	2.1501(26)
				valence sum	1.941(24)
$Co1O_5$ dimers		$Co2O_6$ isolated		$Co3O_6$ chains	
O3-Co1-O3	137.2(9)	O5-Co2-O6	176.7(5)	O1-Co3-O2	82.7(5)
O3-Co1-O4	90.7(8)	O5-Co2-O7	79.3(4) ×2	O1-Co3-O4	96.3(2)
O3-Co1-O9	111.4(8)	O5-Co2-O8	87.7(5) ×2	O1-Co3-O5	169.2(2)
O3-Co1-O9	93.7(2)	O6-Co2-O7	97.8(8) ×2	O1-Co3-O7	101.8(4)
O4-Co1-O9	87.9(8)	O6-Co2-O8	93.7(5)	O1-Co3-O8	80.6(1)
O4-Co1-O9	167.8(4)	O7-Co2-O7	61.7(9)	O2-Co3-O4	170.9(5)
O9-Co1-O9	80.0(5)	O7-Co2-O8	146.5(1) ×2	O2-Co3-O5	95.9(4)
		O7-Co2-O8	85.6(1) ×2	O2-Co3-O7	94.1(3)
		O8-Co2-O8	124.9(3)	O2-Co3-O8	107.6(2)
				O4-Co3-O5	83.2(9)
				O4-Co3-O7	94.8(6)
				O4-Co3-O8	63.4(3)
				O5-Co3-O7	88.9(2)
				O5-Co3-O8	89.6(7)
				O7-Co3-O8	158.2(4)

instance, in KCo one can observe that Co3 (yellow) octahedra chains are joined by isolated Co2 (green) octahedral units. These latter octahedra share two edges with one chain and two vertices with two apical oxygen atoms of the adjacent Co3 chain, thereby forming zigzag layers that extend along the *a* axis. Finally, these layers are joined by the Co1 (pink) dimers, $[Co_2O_9]$ trigonal bipyramids, each sharing an equatorial corner of an opposite Co3 octahedron along the *b* direction.

It is noteworthy that all of the metal cations in KCo are bridged by oxygen, which favours magnetic superexchange interactions. In contrast, the pentagonal sheets in KMn are joined through PO_4 groups, which allows both superexchange and super–superexchange interactions. These differences are responsible for the contrasting magnetic behaviours of these compounds, as is discussed later.

Magnetic properties: Variable-temperature susceptibility measurements on KMn and KCo were carried out on powdered samples in the 4.2–300 K temperature range. Figure 4 shows the temperature dependence of the magnetic susceptibilities and the reciprocal susceptibilities for both compounds.

The thermal evolution of χ_m in KMn follows the Curie–Weiss law, $\chi = C/(T-\theta)$, at high temperatures ($T > 125$ K), with $C_m = 4.43$ emu K mol^{-1} Mn^{2+} and $\theta = -39.06$ K. The experimental effective magnetic moment is 5.89 μ_B per Mn^{2+}, in good agreement with the theoretical value taking into account only the spin contribution. The first signal observed at about 80 K can be attributed to a small amount of Mn_2O_3 as an impurity, as was also detected in the neutron diffraction patterns. This phase shows an antiferromagnetic (AFM) ordering below $T_N = 90$ K.[14] The apparent FM behaviour detected below 100 K is attributed to Mn_3O_4 (not detected in neutron diffraction patterns). On the basis of the susceptibility data for KMn, the amount of impurity was estimated as 0.6% by mass.[15] At low temperature ($T < 20$ K), another magnetic signal appears, centred at 10 K, which may be attributed to 3D AFM ordering of the studied compound.

Different magnetic behaviour is seen for KCo, for which the thermal evolution of χ_m above 20 K follows the Curie–Weiss law with $C_m = 3.64$ emu K mol^{-1} Co^{2+} and $\theta = -22.21$ K. The experimental magnetic moment is 5.39 μ_B per Co^{2+}, in good agreement with the theoretical value, taking into account the unquenched orbital contribution corresponding to the $^4T_{1g}$ term. Below 20 K, the molar susceptibility increases noticeably with decreasing temperature and reaches a maximum value at 7 K, indicating that a long magnetic order is established at this temperature. This behaviour can be attributed to the dominant magnetic exchange interaction of ferromagnetic (FM) character.

In order to clarify the meaning of the above signals, measurements of magnetisation versus magnetic field for the two compounds, obtained at 2 K, are shown in Figure 5. For the KMn derivative, a small hysteresis loop is detected, for which the H_c and M_r values are 200 Oe and 0.028 μ_B, respectively. These results can be interpreted in terms of weak ferromagnetic interactions. On the other hand, for KCo, the

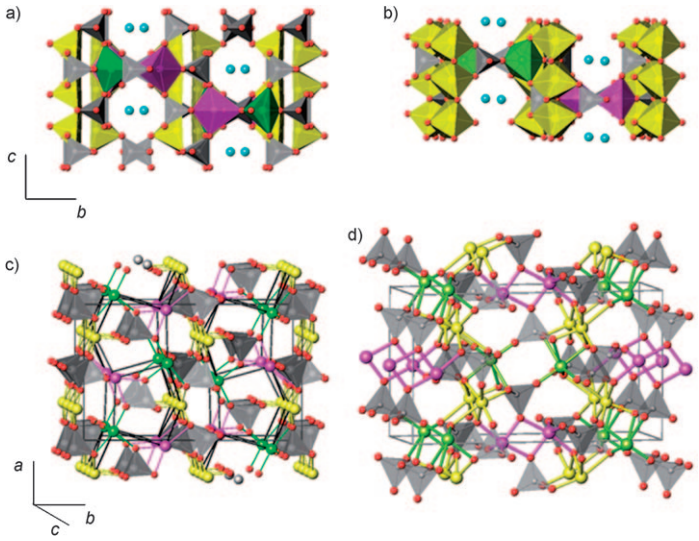

Figure 3. Crystal structure of $KM_4(PO_4)_3$. Projection along the [100] direction for M = Mn (a) and M = Co (b). Projection along the [001] direction for M = Mn (c) and M = Co (d). Colour codes: M1 pink, M2 green, and M3 yellow; PO_4 groups dark-grey tetrahedra; K blue.

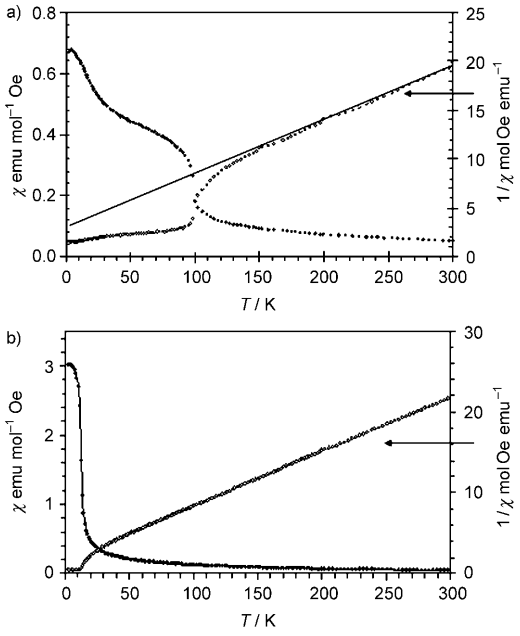

Figure 4. Temperature dependence of molar magnetic susceptibility (χ) and inverse ($1/\chi$) for a) KMn and b) KCo. The apparent FM behaviour of KMn below 100 K is due to an impurity (see text). Note the difference in the scales of χ.

presence of an FM component is confirmed. Thus, the isothermal magnetisation curve corresponding to 2 K shows a remanent magnetisation, its value being around 3.46 μ_B, and a coercitive field of 2500 Oe. This hysteresis loop does not saturate, even at fields as high as 50 kOe, suggesting that an AFM component is also present.

Magnetic structure determination: The thermal evolution of the neutron diffraction pattern (D1B) for $KMn_4(PO_4)_3$ from

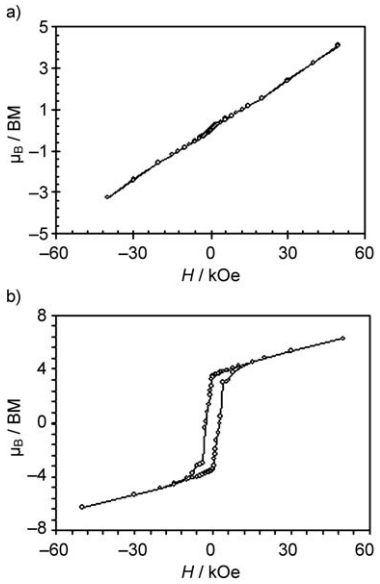

Figure 5. Magnetisation versus magnetic field at 2 K for a) KMn and b) KCo. The curve obtained for KMn clearly indicates antiferromagnetic behaviour and the very weak spontaneous magnetisation is due to an impurity (see text).

1.5 to 100 K is shown in Figure 6. Extra magnetic peaks appear below 10 K and can be attributed to three-dimensional antiferromagnetic ordering in the sample. The intensity of the magnetic reflections increases progressively, reaching a maximum at 1.5 K. The (001) and (003) reflections start to be observed, while others, such as the (101), (102), (111), and (200) reflections, increase in intensity. Thus, the ND patterns at high temperature are characteristic of nuclear scattering alone, and the observed variations should be due to magnetic interactions, in accordance with the above magnetic measurements.

Figure 7 shows the thermal neutron diffraction patterns for $KCo_4(PO_4)_3$ from 2 to 55 K. At around 20 K, noticeable changes in intensity are observed in certain Bragg reflections, all of them allowed in the space group *Pnnm*. In this respect, one can see a noticeable difference between the

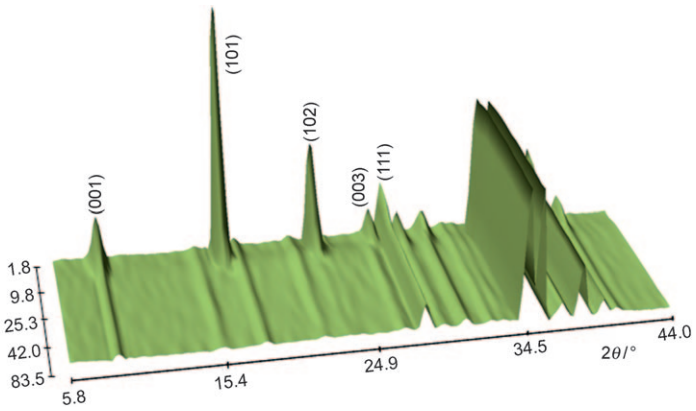

Figure 6. Low-angle part of diffraction patterns for $KMn_4(PO_4)_3$ over a temperature range of 1.8–100 K.

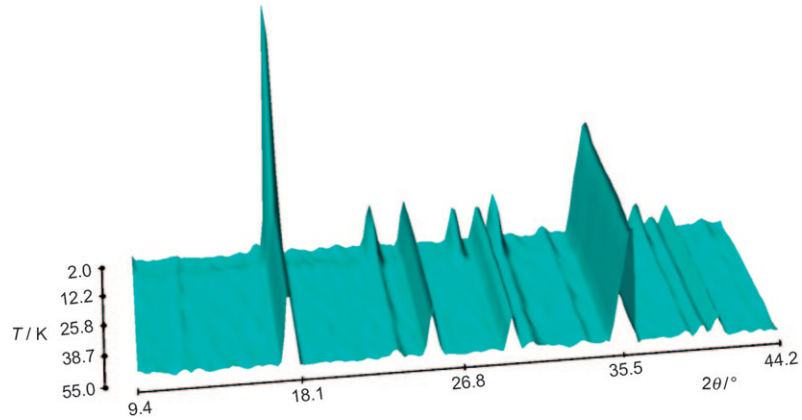

Figure 7. Low-angle part of diffraction patterns for $KCo_4(PO_4)_3$ over a temperature range of 1.8–100 K.

two phosphates, because in the case of KMn some of the above reflections are not permitted in its space group (*Pnam*).

In both cases, the above changes correspond to the onset of magnetic ordering, in accordance with previous studies on a related system [10]. All peaks can be indexed with a propagation vector $\boldsymbol{k}=(0,0,0)$, referred to the reciprocal basis of the room temperature unit cell, indicating that both the magnetic and nuclear cells are similar.

Group theory analysis: The magnetic structures were solved by a systematic search for solutions using the representation symmetry analysis method introduced by Bertaut[16] and extensively developed by Izyumov and co-workers.[17] The possible magnetic structures compatible with the *Pnam* and *Pnnm* space groups and the vector $\boldsymbol{k}=(0, 0, 0)$ were evaluated with the help of the program BasIreps,[18] which allows determination of the symmetry constraints between each magnetic moment of all M^{2+} residing in the same general crystallographic positions. Nevertheless, the present problem is quite complex because the magnetic cations occupy three different crystallographic sites, giving rise to $2\times4 + 8=16$ magnetic sublattices interacting simultaneously. Eight sublattices arise from the general site 8*d* or 8*h* (designated as M3 in Tables 2 and 3 for KMn and KCo, respectively) and the other two four sublattices arise from the special site 4*c* or 4*g* (labelled M1 and M2, respectively). The basis vectors obtained for each irreducible representation Γ_i, according to the projection operator method, are reported in Tables 6 and 7.

The agreement between the observed and calculated diffraction patterns for each possible magnetic structure was tested. After checking all of these solutions, the best fittings were obtained with Γ_8 for Mn and with Γ_7 for Co. The best fit of the D1A experimental pattern at 1.5 K is plotted in Figures 8 and 9. The saturated magnetic moments of all of the cations are given in Table 8.

Table 6. Basis vectors for *Pnam* and $\boldsymbol{k}=0$. Symmetry operators for Mn1 and Mn2: 1. (x, y, z), 2. $(-x, -y, z+1/2)$, 3. $(x+1/2, -y+1/2, -z+1/2)$, 4. $(-x+1/2, y+1/2, -z)$; $\Gamma_m=\Gamma_1+2\Gamma_2+\Gamma_3+2\Gamma_4+2\Gamma_5+\Gamma_6+2\Gamma_7+\Gamma_8$. For Mn3: 1. (x, y, z), 2. $(-x, -y, z+1/2)$, 3. $(x+1/2, -y+1/2, -z+1/2)$, 4. $(-x+1/2, y+1/2, -z)$, 5. $(-x, -y, -z)$, 6. $(x, y, -z+1/2)$, 7. $(-x+1/2, y+1/2, z+1/2)$, 8. $(x+1/2, -y+1/2, z)$[a]; $\Gamma_m=3\Gamma_1+3\Gamma_2+3\Gamma_3+3\Gamma_4+3\Gamma_5+3\Gamma_6+3\Gamma_7+3\Gamma_8$.

	Mn1 and Mn2			Mn3		
	x	*y*	*z*	*x*	*y*	*z*
Γ_1	0	0	C	G+G′	A+A′	C+C′
Γ_2	G	A	0	G−G′	A−A′	C−C′
Γ_3	0	0	F	A+A′	G+G′	F+F′
Γ_4	A	G	0	A−A′	G−G′	F−F′
Γ_5	F	C	0	F+F′	C+C′	A+A′
Γ_6	0	0	A	F−F′	C−C′	A−A′
Γ_7	C	F	0	C+C′	F+F′	G+G′
Γ_8	0	0	G	C−C′	F−F′	G−G′

[a] The notation for the modes for the four sublattices 1, 2, 3, 4 are: F=(+ + + +); A=(+ − − +); G=(+ − + −); C=(+ + − −). The primed modes correspond to the same sequence of signs for the remaining four atoms 4, 5, 6, 7.

Table 7. Basis vectors for *Pnnm* and $\boldsymbol{k}=0$. Symmetry operators for Co1 and Co2: 1. (x, y, z), 2.$(-x, -y, z)$, 3. $(-x+1/2, y+1/2, -z+1/2)$, 4. $(x+1/2, -y+1/2, -z+1/2)$; $\Gamma_m=\Gamma_1+2\Gamma_2+\Gamma_3+2\Gamma_4+2\Gamma_5+\Gamma_6+2\Gamma_7+\Gamma_8$. For Co3: 1. (x, y, z), 2.$(-x, -y, z)$, 3. $(-x+1/2, y+1/2, -z+1/2)$, 4. $(x+1/2, -y+1/2, -z+1/2)$, 5. $(-x, -y, -z)$, 6. $(x, y, -z)$, 7. $(x+1/2, -y+1/2, z+1/2)$, 8. $(-x+1/2, y+1/2, z+1/2)$[a]; $\Gamma_m=3\Gamma_1+3\Gamma_2+3\Gamma_3+3\Gamma_4+3\Gamma_5+3\Gamma_6+3\Gamma_7+3\Gamma_8$.

	Co1 and Co2			Co3		
	x	*y*	*z*	*x*	*y*	*z*
Γ_1	0	0	C	A+A′	G+G′	C+C′
Γ_2	A	G	0	A−A′	G−G′	C−C′
Γ_3	0	0	F	G+G′	A+A′	F+F′
Γ_4	G	A	0	G−G′	A−A′	F−F′
Γ_5	C	F	0	C+C′	F+F′	A+A′
Γ_6	0	0	A	C−C′	F−F′	A−A′
Γ_7	F	C	0	F+F′	C+C′	G+G′
Γ_8	0	0	G	F−F′	C−C′	G−G′

[a] The notation for the modes for the four sublattices 1, 2, 3, 4 are: F=(+ + + +); A=(+ − − +); G=(+ − + −); C=(+ + − −). The primed modes correspond to the same sequence of signs for the remaining four atoms 4, 5, 6, 7.

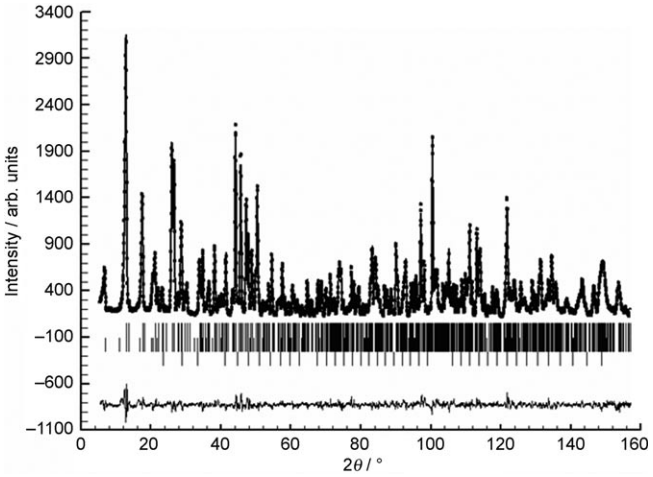

Figure 8. Observed and calculated neutron diffraction patterns of $KMn_4(PO_4)_3$ at 1.5 K and the difference between them.

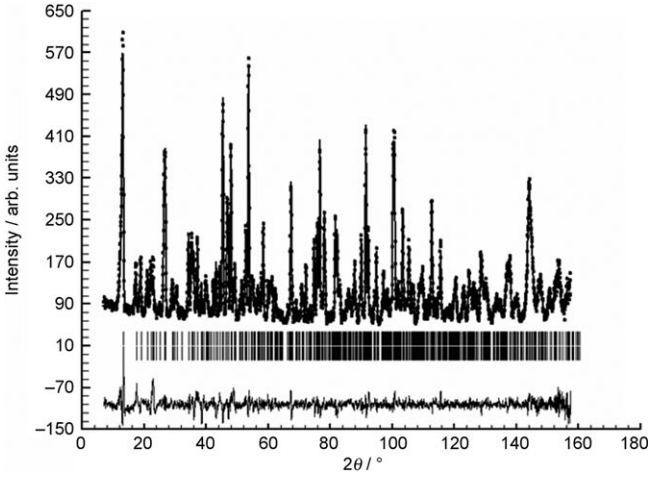

Figure 9. Observed and calculated neutron diffraction patterns of $KCo_4(PO_4)_3$ at 1.5 K and the difference between them.

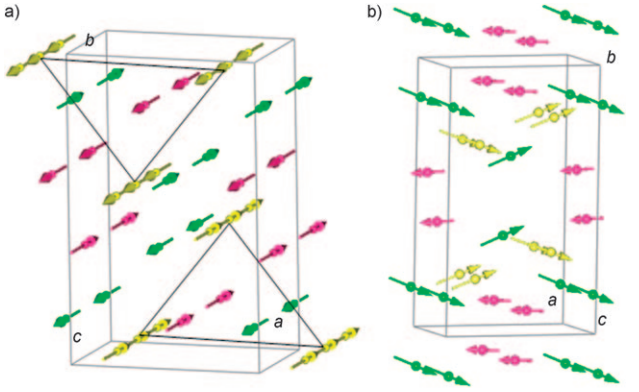

Figure 10. Magnetic structure model showing the three transition metal sites and their respective magnetic moments: a) $KMn_4(PO_4)_3$ and b) $KCo_4(PO_4)_3$.

Table 8. Magnetic moments and discrepancy factors associated with the models for $T=2$ K for $KM_4(PO_4)_3$ (M = Mn[a] and Co[b]).

	G_z		F_x	C_y	G_z	μ (μ_B)
Mn1	+4.43	Co1	−2.16	+0.10	–	2.16
Mn2	−4.21	Co2	+2.80	−1.51	–	3.18
Mn3	−4.57	Co3	+2.94	+1.11	0	3.14

[a] $R_p=4.81$; $R_{wp}=6.10$, $\chi^2=3.9$, $R_B=3.90$, and $R_{mag}=4.58$. [b] $R_p=5.32$; $R_{wp}=6.85$, $\chi^2=2.4$, $R_B=4.58$, and $R_{mag}=7.99$.

The refined magnetic structural model of $KMn_4(PO_4)_3$, corresponding to the representation Γ_8 of *Pnam* for $\boldsymbol{k}=0$, is depicted in Figure 10a). As previously pointed out, the crystal structure consists of an arrangement of three types of entities sharing corners: Mn1 (pink) and Mn2 (green) polyhedra, which are mutually isolated, and Mn3 (yellow) square-pyramidal chains extending parallel to the *y* direction. In the magnetic structure, all of these entities are ferromagnetically ordered along the *c* direction. A striking feature is that three chains of Mn3 with the same spin orientation are arranged in nearly equilateral triangles, the bases of which are in the *xz* plane, and these triangles are superimposed with antiparallel magnetic moment orientations in the *y* direction. Within the vertical limits of these triangles, the Mn1 and Mn2 chains are mutually AFM coupled in the same plane, showing an antiparallel orientation of the Mn2 ions with respect to the others. Therefore, there are FM layers of Mn3, with the Mn1 and Mn2 between them and showing AFM interactions. As can be seen in Table 6, the representation Γ_8 does not allow FM components, so the very weak ferromagnetism seen in the magnetisation curve of Figure 5a is certainly due to impurities.

The magnetic ordering of $KCo_4(PO_4)_3$, corresponding to the representation Γ_7 of *Pnnm* for $\boldsymbol{k}=0$, is depicted in Figure 10b). In this perspective, the octahedral Co3 (yellow) chains show an FM component along the *x* direction; with respect to the *y* component, the magnetic structure consists of FM chains that are antiferromagnetically coupled. Between these Co3 chains, the Co2 (green) isolated octahedra are ferromagnetically coupled along the *x* direction; in contrast, along the *y* direction the coupling is FM with one of the Co3 chains and AFM with the other. Finally, the Co1 (pink) trigonal dimers are ferromagnetically ordered along the *x* direction, being also antiferromagnetically coupled with the Co3 chains. As can be seen in Table 7, the representation Γ_7 allows FM components along the *x* direction. This is in complete agreement with the ferromagnetism seen in the magnetisation curve of Figure 5b).

Discussion

The above structural models allow one to interpret the respective magnetic behaviours of the studied compounds,

which were found to be AFM in the KMn phosphate and FM with an AFM component in the KCo phosphate. This latter behaviour was also encountered in the isostructural nickel phosphate, with neither of these compounds being collinear, with spin modes (F_x,C_y,0) and (C_x,F_y,0), respectively. The different spin direction in $KCo_4(PO_4)_3$ is probably due to the high contribution of magnetic anisotropy of the Co^{2+} cations as compared to that of the more isotropic Ni^{2+} cations.

The changes observed in the neutron diffraction patterns at 10 K (see Figures 6 and 7) are clearly due to the establishment of long-range AFM ordering in the KMn derivative and FM ordering in the KCo analogue. The magnetic moments obtained at 1.5 K in KMn (4.43 μ_B for Mn1, 4.21 μ_B for Mn2, and 4.57 μ_B for Mn3) are less than 85% of the spin-only moment of Mn^{2+} ions. A reduction to the spin-only values of free ions is normally due to a combination of covalence effects and zero-point spin fluctuations in antiferromagnets.[19] The magnetic moments obtained in KCo (3.18 and 3.14 μ_B for Co2 and Co3, respectively) are slightly higher than the maximum value of 3 μ_B expected for the electronic configuration of a high-spin Co^{2+} free ion ($3d^7$, $t_{2g}^5e_g^2$). This slightly overestimated value may be due to the well-known fact that this ion in its high-spin state exhibits relatively strong spin-orbit coupling and an orbital contribution to the magnetic moment.[20] This is also the physical origin of the strong single-ion anisotropy shown by Co^{2+} in many oxides. This particular anisotropy also accounts for the different magnetic structure observed for $KCo_4(PO_4)_3$ as compared with the Ni phosphate. Finally, we note that the refined magnetic moments of the Co2 and Co3 octahedral ions are always higher than that of the bipyramidal-trigonal Co1.[3]

Spontaneous static ordering of magnetic moments at low temperatures is caused by exchange interactions between the moments, making it energetically favourable for them to align in a parallel or anti-parallel manner. To study the main characteristics of the magnetic ordering in these phases, only isotropic exchange interactions were taken into account. The anisotropic terms, which act as a perturbation fixing the orientation of the spins with respect to crystallographic lattice, were taken to be negligible. The possible competition between exchange and anisotropy may play a non-negligible role in the case of the Co compound, giving rise to the observed non-collinear structure.

Analysis and discussion of the magnetic structure of $KMn_4(PO_4)_3$: The magnetic ions interact through super or super-superexchange mediated by oxygen ions, all of them belonging to discrete tetrahedral PO_4 anions. The nature of these interactions between two Mn^{2+} (d^5–d^5) ions should be antiferromagnetic at 180° and ferromagnetic for an angle of 90°, in accordance with the Goodenough–Kanamori–Anderson (GKA) rules.[21–23]

Analysis of the crystal structure of $KMn_4(PO_4)_3$ allows us to establish several main exchange pathways (see Figure 11):

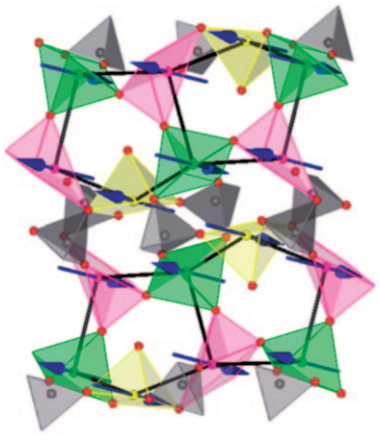

Figure 11. Exchange pathway for $KMn_4(PO_4)_3$. Interactions via vertex oxygen bridges and phosphate groups.

- The shortest path (Mn3–Mn3 (yellow) = 3.23 Å) is of a superexchange type; the Mn^{2+} ions belong to the same chains and the Mn-O-Mn angles of 97.5° indicate, according to the GKA rules, an FM exchange pathway.
- Superexchange paths are operative between Mn3 (yellow)–Mn1 (pink) and Mn3 (yellow)–Mn2 (green); the bond lengths between the cations are 3.55 and 3.82 Å, respectively. The Mn3-O-Mn1 and Mn3-O-Mn2 angles are 102 and 119°, respectively. According to the GKA rules, these angles are close to the threshold between FM and AFM coupling; the first corresponds to a weak FM exchange and the second to weak AFM exchange.
- The Mn2 (green)–Mn1 (pink) distances are 3.92 Å and 3.99 Å. Superexchange interactions between [$Mn2O_5$] and [$Mn1O_5$] polyhedra may be operative through the O9 and O7 atoms, with angles of 133 and 139°, respectively. Therefore, AFM interactions between them are expected.
- The Mn^{2+} ions of different pentagonal sheets are connected by PO_4 groups, and therefore super-superexchange interactions through [$P1O_4$] or [$P2O_4$] could be operative. In these cases, the angles are always greater than 120°, and therefore AFM couplings are favourable.

Figure 12 shows the magnetic structure, together with the coordination polyhedra, for the manganese compound. The Mn^{2+} ions form pentagons, which extend in a zigzag manner along the *a* direction and in a parallel manner along *c*, and are AFM or FM coupled (Mn3–Mn1). These pentagonal blocks are linked along the *b* direction to other similar blocks through isolated [PO_4] groups. Therefore, the only possible pathway between the above *ac* layers is the super-superexchange interaction. This situation produces a change in the signs of the magnetic moments orientation in Mn chains. As a consequence, successive pentagons along *b* are reverse images of the previous ones. This AFM structure is in complete agreement with the results obtained from the magnetic measurements and with the predictions of the

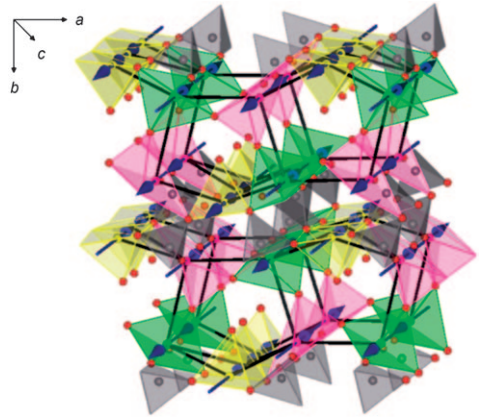

Figure 12. Magnetic structure of $KMn_4(PO_4)_3$.

qualitative analysis of the exchange interactions using the GKA rules described in the previous paragraph.

Analysis and discussion of the magnetic structure of $KCo_4(PO_4)_3$: By means of an analogous procedure to that discussed above, the main magnetic exchange pathways in $KCo_4(PO_4)_3$ have been identified as the following (see Figure 13):

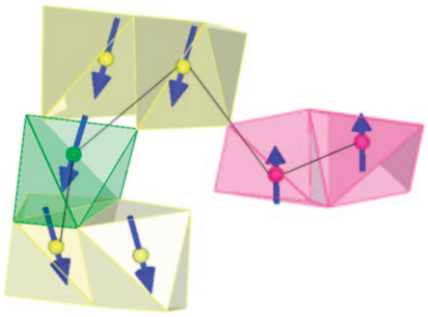

Figure 13. Exchange pathway for $KCo_4(PO_4)_3$. Interactions via vertex oxygen bridges.

- The shortest path (Co3 (yellow)–Co3 (yellow) = 2.94 Å) is of a superexchange type; the Co^{2+} ions belong to the same chains and the Co-O-Co angles of 93.5° correspond, according to the GKA rules, to an FM exchange pathway.
- Superexchange intradimer interactions through oxygen atoms involving metal $d_{x^2-y^2}$ orbitals from edge-sharing cobalt polyhedra in ($Co1_2O_8$) trigonal-bipyramidal dimers, in which the Co-O-Co angles are 98.8°, give rise to FM coupling.
- The interactions between Co3 (yellow)–Co2 (green) with distances of 3.15 and 3.71 Å, respectively, are of a superexchange type. Superexchange interactions between ($Co3O_8$) chains and ($Co2O_6$) isolated octahedral may operate through the O5 and O8 atoms, the former providing the greatest opportunity for orbital overlap, Co3-O5-Co2 (bond lengths 2.15, 2.09 Å and angle 95.5°). Therefore, FM interactions are to be expected.
- The distance between Co3 (yellow) and Co1 (pink) is 3.69 Å and superexchange interactions between [$Co3O_6$] and [$Co1O_5$] polyhedra may operate through the O4 atoms, with angles of 118°. Therefore, AFM interactions are to be expected in this case.

Figure 14 shows the final magnetic structure of the KCo phosphate, in which Co1 (pink) dimers seem to be responsible for FM couplings between Co3 (yellow) chains, which give rise to a global FM response with a spontaneous net magnetisation.

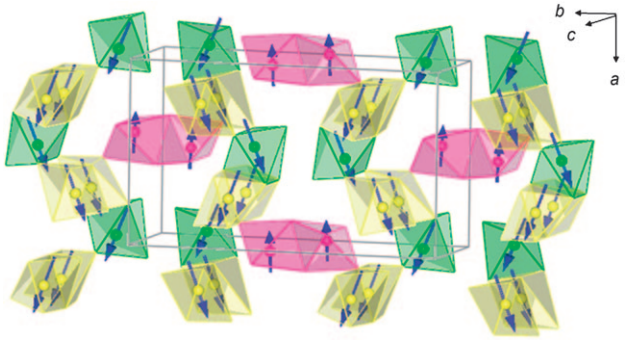

Figure 14. Magnetic structure of $KCo_4(PO_4)_3$.

Conclusion

We have solved and refined the magnetic structures of two orthophosphates, $KMn_4(PO_4)_3$ and $KCo_4(PO_4)_3$, the crystal structures of which are closely related. These systems show complex interactions between the magnetic ions. Different magnetic orderings are set up below the respective Néel temperatures, both of which are close to $T_N = 10$ K. In the manganese phosphate, three kinds of Mn^{2+} cations are ferromagnetically ordered in parallel infinite chains along the *c*-direction and are mutually antiferromagnetically and ferromagnetically coupled through superexchange interactions. The most prominent aspect of the magnetic topology of $KMn_4(PO_4)_3$ is the arrangement of such chains in nearly planar pentagonal rings of Mn^{2+} ions. These rings share edges in the *ab* plane, giving rise to double layers along the *ac* plane. It is noteworthy that the Mn^{2+}–Mn^{2+} magnetic interactions between parallel layers are of the super-superexchange type through [PO_4] anions and are of weak AFM character. The main consequence of this coupling is the inversion of spin moment alignment in each chain. As a result, the global magnetic structure is purely AFM.

The $KCo_4(PO_4)_3$ derivative is isostructural with the nickel phosphate of the same stoichiometry, but shows a different spin orientation that may be attributed to the single-ion anisotropy contribution of Co^{2+}. The competition between anisotropy and exchange is probably the origin of the non-collinear magnetic structure in this case. The main feature is

the FM character of the Co3 chain polyhedra, which differs from that encountered in the manganese derivative with both FM and AFM couplings for the Mn cations with the same label (i.e., Mn1–Mn1, Mn2–Mn2, Mn3–Mn3). Superexchange interactions starting from ferromagnetically coupled Co2 dimers are responsible for the overall FM character of this phosphate.

Experimental Section

Polycrystalline samples of $KM_4(PO_4)_3$ (M = Mn and Co) were obtained by the "liquid mix" technique[11] from powdered mixtures of KNO_3, $C_{10}H_{14}MnO_4$, $Co(NO_3)_2{\cdot}6H_2O$, and $(NH_4)_2HPO_4$ (supplied by Merck, Germany), in stoichiometric ratios. The reactants were heated in an alumina crucible at temperatures above 1100 K for 24 h.

Neutron diffraction patterns were recorded at room temperature and 2 K on a D1A high-resolution diffractometer at the ILL (Grenoble, France). A wavelength of 1.911 Å was selected by means of a germanium monochromator. The counting time was 6 h using about 4 g of sample contained in a vanadium can. Diffraction patterns were analysed using the FullProf program.[12] A D1B powder diffractometer, equipped with a PSD multidetector and a pyrolitic graphite monochromator providing a wavelength of 2.52 Å, was used to obtain diffraction patterns in the temperature range 1.5–300 K.

Magnetic susceptibility data were measured with a SQUID magnetometer (Quantum Design, MPMS-XL model) in the temperature range 1.9–300 K at different applied fields. Isothermal magnetisation measurements were made at up to 60 kOe at different temperatures.

Acknowledgements

Financial support through research Project MAT2006–10021 (CICYT) and CCG06-UCM/MAT-1333 (UCM-CAM, Spain) is acknowledged. We also thank Dr. Gabriel Cuello for assistance with the D1A and D1B diffractometers and the ILL facilities.

[1] J. Escobal, J. L. Pizarro, J. L. Mesa, J. M. Rojo, B. Bazan, M. I. Arriortua, T. Rojo, *J. Solid State Chem.* **2006**, *179*, 2626–2634.
[2] J. Escobal, J. L. Pizarro, J. L. Mesa, A. Larrañaga, J. Rodríguez-Fernández, M. I. Arriortua, T. Rojo, *J. Solid State Chem.* **2006**, *179*, 3052–3058.
[3] J. M. Rojo, J. L. Mesa, L. Lezama, J. L. Pizarro, M. I. Arriortua, J. Rodríguez-Fernández, G. E. Barberis, T. Rojo, *Phys. Rev.* **2002**, *B66*, 094406.
[4] E. N. Matvienko, O. V. Yakubovich, M. A. Simonov, N. V. Belov, *Sov. Phys. Dokl.* **1981**, *26*, 633–635.
[5] M. Ben Amara, M. Vlasse, R. Olazcuaga, G. Le Flem, P. Hagenmuller, *Acta Crystallogr. Sect. C* **1983**, *39*, 936–939.
[6] J. B. Anderson, J. Moring, E. Kostiner, *J. Solid State Chem.* **1985**, *60*, 358–365.
[7] O. V. Yakubovich, O. A. Evdokimona, O. K. Mel′nikov, M. A. Simonov, *Sov. Phys. Crystallogr.* **1986**, *31*, 151.
[8] A. Daidouh, C. Pico, M. L. Veiga, *Solid State Ionics* **1999**, *124*, 109–117.
[9] S. Neeraj, M. L. Noy, A. K. Cheetham, *Solid State Sci.* **2002**, *4*, 397–404.
[10] M. L. López, C. Durio, A. Daidouh, C. Pico, M. L. Veiga, *Chem. Eur. J.* **2004**, *10*, 1106–1113.
[11] M. Pechini, US Patent 3231328, **1996**.
[12] J. Rodríguez-Carvajal, *Physica B* **1993**, *192*, 55. The programs of the *FullProf Suite* and their corresponding documentation can be obtained from the Web at http://www.ill.eu/sites/fullprof/. The drawings of crystal and magnetic structures have been generated using the program *FullProf Studio* by L. C. Chapon and J. Rodríguez-Carvajal (unpublished). *FullProf Studio* is a program of the *FullProf Suite*.
[13] R. D. Shannon, *Acta Crystallogr. Sect. A* **1976**, *32*, 751–753.
[14] M. Regulski, R. Przenioslo, I. Sosnowska, D. Hohlwein, R. Schneider, *J. Alloys Compd.* **2004**, *362*, 236–240.
[15] L. Ortega-San Martín, J. P. Chapman, L. Lezama, J. Sanchez-Marcos, J. Rodríguez-Fernández, M. I. Arriortua, T. Rojo, *Eur. J. Inorg. Chem.* **2006**, 1362–1370.
[16] E. F. Bertaut, *Acta Crystallogr. Sect. A* **1968**, *24*, 217–231.
[17] Y. A. Izyumov, V. E. Naish, R. P. Ozerov, *Neutron Diffraction of Magnetic Materials*, Consultants Bureau, New York, **1991**.
[18] J. Rodríguez-Carvajal, BasIreps Program (unpublished). This program is part of the *FullProf Suite* (see ref. [12]).
[19] N. El Khayati, J. Rodríguez-Carvajal, F. Bourée, T. Roisnel, R. Cherkaoui, A. Boutfessi, A. Boukhari, *Solid State Sci.* **2002**, *4*, 1273–1283.
[20] G. Rousse, J. Rodríguez-Carvajal, S. Patoux, C. Masquelier, *Chem. Mater.* **2003**, *15*, 4082–4090.
[21] J. B. Goodenough, *Magnetism and the Chemical Bond*, Interscience, New York, **1963**.
[22] J. Kanamori, *J. Phys. Chem. Solids* **1959**, *10*, 87.
[23] P. W. Anderson, in *Magnetism, Vol. I* (Eds.: G. T. Rado, H. Suhl), Academic Press, New York, **1963**, p. 67.

Received: April 22, 2008
Published online: October 16, 2008

